AGU PUBLICATIONS

Geophysical Research Letters

RESEARCH LETTER
10.1002/2016GL068238

Key Points:
- A novel method objectively quantifies the shape of nonstationary meanders over all spatial scales
- A tree made from the wavelet transform (WT) of curvature captures the spatial structure of meanders
- The WT at the submeander scale results in two simple shape parameters: fattening and skewing

Supporting Information:
- Supporting Information S1

Correspondence to:
B. Vermeulen,
bart.vermeulen@wur.nl

Citation:
Vermeulen, B., A. J. F. Hoitink, G. Zolezzi, J. D. Abad, and R. Aalto (2016), Multiscale structure of meanders, *Geophys. Res. Lett.*, *43*, doi:10.1002/2016GL068238.

Received 11 FEB 2016
Accepted 10 MAR 2016
Accepted article online 16 MAR 2016

Multiscale structure of meanders

B. Vermeulen[1], A. J. F. Hoitink[1], G. Zolezzi[2], J. D. Abad[3], and R. Aalto[4]

[1]Department of Environmental Sciences, Wageningen University, Wageningen, Netherlands, [2]Department of Civil, Environmental and Mechanical Engineering, University of Trento, Trento, Italy, [3]Department of Civil and Environmental Engineering, University of Pittsburgh, Pittsburgh, Pennsylvania, USA, [4]Geography, College of Life and Environmental Sciences, University of Exeter, Exeter, UK

Abstract River meander planforms can be described based on wavelet analysis, but an objective method to identify the main characteristics of a meander planform over all spatial scales is yet to be found. Here we show how a set of simple metrics representing meander shape can be retrieved from a continuous wavelet transform of a planform geometry. We construct a synoptic multiple looping tree to establish the meander structure, revealing the embedding of dominant meander scales in larger-scale loops. The method can be applied beyond the case of rivers to unravel the meandering structure of lava flows, turbidity currents, tidal channels, rivulets, supraglacial streams, and extraterrestrial flows.

1. Introduction

Meandering is a common geophysical process that is often described in fluvial context, while it can be the consequence of a wide variety of processes occurring on earth, including (submarine) lava flows [*Fornari*, 1986], submarine turbidity currents [*Peakall et al.*, 2000; *Abreu et al.*, 2003; *Kolla et al.*, 2007], tidal channels [*Marani et al.*, 2002], rivulets [*Le Grand-Piteira et al.*, 2006], supraglacial streams [*Karlstrom et al.*, 2013], and on the surface of other planets in the solar system [*Greeley*, 1971; *Komatsu and Baker*, 1994; *Baker*, 2001; *Malin and Edgett*, 2003]. Several underlying processes and principles governing meander shape have been proposed and may include the following: self-organization [*Hooke*, 2007], flow dynamics [*Seminara*, 2006], directed Brownian walk [*Lazarus and Constantine*, 2013], heritage from older geomorphological forms [*Harden*, 1990] and substrate heterogeneity [*Güneralp and Rhoads*, 2011; *Motta et al.*, 2012, 2014], but the parametric description of meander shape remains an important challenge in geomorphology [*Schumm*, 1967], environmental engineering [*Rinaldi and Johnson*, 1997], and climate studies [*Stark et al.*, 2010].

The large complexity of a meander train is reflected in upstream or downstream skewness [*Parker et al.*, 1983; *Seminara et al.*, 2001; *Marani et al.*, 2002; *Güneralp and Rhoads*, 2011] or fattening [*Parker et al.*, 1982, 1983], curvature peaks [*Vermeulen et al.*, 2014, 2015], compound loops [*Brice*, 1974; *Frothingham and Rhoads*, 2003; *Hooke*, 2003] and double heading [*Thompson*, 1986]. Quantifying all of these planform characteristics is a challenging task due to nonstationarity and the multiscale nature of meander planform geometry. Until now most techniques are only in part suitable to determine the shape of meanders or are unsuitable to quantify meander characteristics [*Hooke*, 1984]. These techniques often focus on different scales, typically the meander scale, valley scale, or more recently also a cutoff scale or mean center scale [*Gutierrez and Abad*, 2014].

Typical measures to characterize meanders are sinuosity and meander wavelength. In a multiscale planform the value of sinuosity will depend on the scale at which the meandering feature is analyzed [*Andrle*, 1996]. Determining meander wavelength involves the detection of inflection points of the planform [*Howard and Hemberger*, 1991] (corresponding to zero crossings in curvature), which is a subjective process that can suffer from irregularities in meander shape and sampling of the planform [*Andrle*, 1996]. An alternative approach is to consider the direction change of a planform at fixed distances [*O'Neill and Abrahams*, 1986]. This methodology, however, cannot accommodate processes at different scales. The angle change can also be observed at different scales [*Andrle*, 1996], but the neglect of nonstationarity remains. The result of this latter technique is similar to what is obtained by applying Fourier Transforms to curvature series. This can be done on a meander by meander basis [*Marani et al.*, 2002], which, however, involves the detection of inflection points first. More recently, the use of wavelet transforms of curvature series has been employed to describe meandering behavior to detect changes in meandering characteristics [*van Gerven and Hoitink*, 2009], analyzing the

change at different supermeander scales [*Gutierrez and Abad*, 2014], and to characterize the wavelengths of meandering [*Zolezzi and Güneralp*, 2015].

Wavelet transforms have the potential to objectively characterize meanders and have been widely applied for geophysical studies [*Foufoula-Georgiou and Kumar*, 1994; *Nicolleau and Vassilicos*, 1999; *Beyer*, 2003; *Lashermes et al.*, 2007; *Hardy et al.*, 2009; *Yuan et al.*, 2009; *Mount et al.*, 2013; *Gutierrez and Abad*, 2014; *Keylock et al.*, 2014; *Koenders et al.*, 2014]. In the field of pattern recognition, scale space images, close relatives of the wavelets, are widely applied to describe the multiscale structure of planar curves and images [*Witkin*, 1984; *Yuille and Poggio*, 1986; *Mackworth and Mokhtarian*, 1988; *Lowe*, 1989; *Lindeberg*, 1990; *Mokhtarian and Mackworth*, 1992; *Rosin*, 1998]. Scale space images or wavelets are well described by zero crossings [*Mallat*, 1991; *Rosin*, 1998] and wavelet modulus maxima [*Muzy et al.*, 1993], which can be used to construct scale space trees [*Witkin*, 1984; *Jaffard*, 1996] and unravel the multifractal structure of the underlying signal [*Muzy et al.*, 1991; *Nicolleau and Vassilicos*, 1999].

In this contribution we propose a quantitative method based on continuous wavelet transforms to study the planform shape of meandering features, which is able to capture the meander characteristics from the submeander scale to the largest valley line scale, using zero crossings and local peaks in the wavelet spectrum. After defining the curvature (section 2.1), a continuous wavelet transform is computed (section 2.2) and used as a basis to construct a scale space tree (section 2.3). The scale space tree is used to identify half meanders and multiple loops (section 2.4). Eventually, the shape of the meanders is quantified by two parameters (section 2.5). The method is tested on synthetic planforms (section 3.1) and four rivers (section 3.2) followed by the conclusions (section 4) of this work.

2. Method

Meander planforms are multiscale, nonstationary features. Therefore, they are analyzed on the basis of a continuous wavelet transform (CWT) of their curvature. Peaks in the wavelet spectrum are detected and hierarchically ordered in a tree. The tree is crossed from smallest to largest scales to identify the most powerful peaks that define the local scale and location of meanders. Detected meanders are linked to larger-scale structures, or multiple loops, through the tree. The wavelet spectrum at submeander scales characterizes meander shape that is quantified with two parameters: skewing and fattening.

2.1. Curvature

The x and y coordinates of a meander are nondimensionalized as follows:

$$\hat{x} = \frac{x - x_0}{W}, \quad \hat{y} = \frac{y - y_0}{W} \tag{1}$$

where x_0 and y_0 are the starting x and y coordinates of the planform, respectively, and W is the average width of the meandering form. $\hat{x}$ and $\hat{y}$ can be expressed as a function of the distance along the planform, nondimensionalized with the width, $\hat{s} = s/W$. The nondimensional curvature (C) of the planform is the ratio of the width and the inverse of the local radius of curvature (R) and is computed as

$$C = \frac{W}{R} = \frac{\frac{\mathrm{d}\hat{x}}{\mathrm{d}\hat{s}}\frac{\mathrm{d}^2\hat{y}}{\mathrm{d}\hat{s}^2} - \frac{\mathrm{d}\hat{y}}{\mathrm{d}\hat{s}}\frac{\mathrm{d}^2\hat{x}}{\mathrm{d}\hat{s}^2}}{\left(\left(\frac{\mathrm{d}\hat{x}}{\mathrm{d}\hat{s}}\right)^2 + \left(\frac{\mathrm{d}\hat{y}}{\mathrm{d}\hat{s}}\right)^2\right)^{\frac{3}{2}}} \tag{2}$$

Equation (2) is less sensitive to noise in the input coordinates when the derivatives are approximated with centered differences [cf. *Schwenk et al.*, 2015]. The calculation of curvature is notably affected by noise and often requires some level of smoothing. In this study such smoothing is not necessary, since the wavelet transform is essentially smoothing the curvature series at different scales. All planforms were sampled with a resolution of one fifth of the width, enough to identify smaller-scale oscillations.

2.2. Continuous Wavelet Transform

The obtained curvature series are transformed with a continuous wavelet transform (CWT). The resulting CWT is strongly determined by the choice of mother wavelet [*Torrence and Compo*, 1998]. This choice is a trade-off between spatial resolution and scale resolution. A high spatial resolution has the advantage to better distinguish different features in space. Another important choice to be made is whether to use real or complex wavelets. Complex wavelets are more suitable for periodic behavior and detection of phase changes while

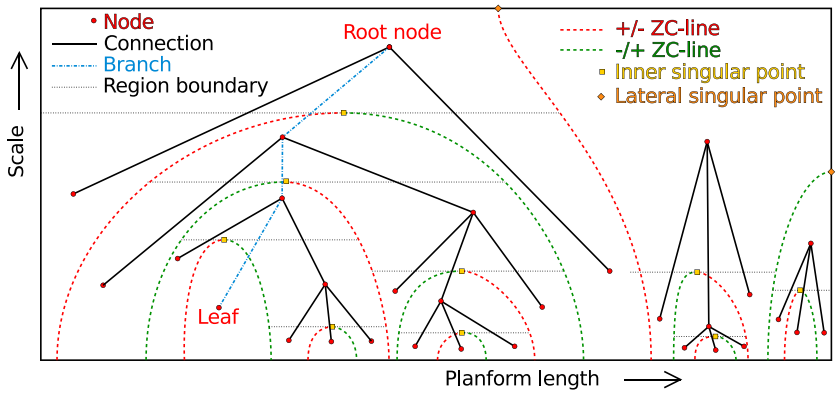

Figure 1. Illustration of zero crossing lines extracted from the CWT and the corresponding ternary tree with a definition of the terminology used.

real wavelets are more suitable to detect abrupt changes in amplitude [*Torrence and Compo*, 1998]. A main difference between complex and real wavelets is that the latter can distinguish between single peaks, which in the case of a planform means being able to distinguish between different half meanders. The wavelet transform can be either positive or negative, depending on the curvature direction of the planform. In this analysis we chose for the derivative of Gaussian wavelet of order 2, commonly known as the "Mexican-hat" wavelet. This wavelet was chosen since it is a real-valued wavelet particularly suited for the detection of peaks in the original signal [*Torrence and Compo*, 1998] and with a good trade-off between spatial localization and spectral resolution. Since the wavelet is a second order derivative of a Gaussian, the wavelet transform of the curvature will be a scale representation of the second derivative of the curvature. This allows to better detect small peaks at scales smaller than the meander scale. The resulting wavelet transform is a two-dimensional plane which is a function of the spatial coordinate (the *s* coordinate) and the scale of fluctuation. We will call this the CWT plane. The limits of the CWT plane are given laterally by the minimum and maximum spatial coordinate and vertically by the smallest and largest scale.

2.3. Scale Space Trees

The curvature signal and its main features are well characterized by the zero crossing (ZC) lines of the CWT plane [*Mallat*, 1991]. Pairs of ZC lines emerge at singular points within the CWT plane (Figures 1 and S1 in the supporting information), while single ZC lines emerge at singular points at the sides of the plane (Figures 1 and S1). The ZC lines leave the CWT plane at the smallest scales nearly orthogonal to the *s* axis (Figures 1 and S1). The ZC lines partition the CWT plane in regions (Figure 1) which define a ternary tree, often referred to as the scale space tree [*Witkin*, 1984; *Muzy et al.*, 1991; *Jaffard*, 1996; *Rosin*, 1998; *Jaffard et al.*, 2007]. The regions are laterally confined by the ZC lines and vertically by singular points (Figure 1). The root regions, which represent the root nodes [*Harris et al.*, 2008] of the ternary trees, are bounded on the large-scale side of the plane by singular points at the sides of the CWT plane (Figure S1). On the small-scale side the regions are bounded by singular points within the CWT plane where pairs of ZC lines emerge. These lines split the parent region in three new, smaller-scale regions. These regions are represented in the tree as three child nodes of the root node. This process is repeated recursively until the smallest scales are reached, partitioning the entire CWT plane in regions, which are organized in the scale space trees. The scale space tree forms the basis to identify half meanders.

2.4. Meander and Multiple Loop Identification

Half meanders are identified based on local peaks (minima and maxima) in the CWT plane. The basic idea of the method, which will be described in more technical detail below, is that each fluctuation in the curvature series at the smallest scales is embedded in a train of fluctuations of increasingly large scale. The most powerful peak in this train of fluctuations defines the half meander. These half meanders are embedded in the train of larger-scale fluctuations, which are called "multiple loops" since they contain several smaller-scale oscillations. All curvature fluctuations at smaller scales than the half meander scale are used to determine the meander shape (section 2.5).

The train of curvature fluctuations from small-scale to large-scale is represented in the tree by a series of nodes connecting the smallest-scale node (smallest-scale fluctuation in curvature) to the corresponding root node

at the largest-scale (largest-scale fluctuation in the curvature series). This series of nodes is called a "branch" (Figure 1). The most powerful nodes and therefore the most powerful curvature fluctuations are identified as a meander node and correspond to a half meander or bend. All parent nodes of the meander node are defined as "multiple loop" nodes. All child nodes of a meander node are removed from the tree. The resulting tree connects the meander nodes at the smallest scales to the large-scale fluctuations and is called the "multiple loop tree." This tree represents how meanders are embedded in larger-scale loops of the planform.

The planform reaches corresponding to the meander nodes and multiple loop nodes are determined by the spatial position of the bounding ZC lines at the scale of the local peak. These reaches correspond to a half meander or a single bend, in the case of a meander node. The portion of the CWT plane at scales smaller than the meander scale determine the shape of the meander. This part of the CWT plane will be used to determine the shape parameter in section 2.5.

The local peaks in the CWT plane that identify half meanders are detected with a hexagonal lattice, a robust technique to detect extremes and saddle points on 2-D surfaces [*Kuijper*, 2004]. In regions having more than one peak, only the strongest peak is considered. Regions without local peaks are removed from the tree. It can happen in the process described above, that a node identified as meander node also belongs to a branch in which it is identified as a multiple loop node. To overcome this issue, the process is repeated, keeping track of all multiple loop nodes, which are not anymore allowed to be meander nodes in other branches. Once no new multiple loop nodes are found the process ends.

2.5. Meander Shape Parameterization

The CWT at scales smaller than the meander scale characterize the shape of the meander. A frequently used shape of river planforms is generated with the Kinoshita curve [*Parker et al.*, 1983]. The Kinoshita curve gives the angle of the planform as a function of the s coordinate:

$$\theta(s) = \theta_0 \cos\phi - \theta_0^3 \left(c_f \cos(3\phi) + c_s \sin(3\phi)\right) \tag{3}$$

in which θ_0 is the amplitude of the planform angle and $\phi = 2\pi s/\lambda_m$, where λ_m is a typical meander wavelength. The parameters c_f and c_s account for fattening and skewing of meanders, respectively.

The Kinoshita curve can help to identify the effect of certain shapes on the spectral response of the curvature series. The curvature generated by the Kinoshita is

$$C(s) = W\frac{d\theta(\hat{s})}{d\hat{s}} = \\ = -\frac{2\pi W}{\lambda_m}\left(\theta_0 \sin\phi + 3\theta_0^3(c_s f_S - c_f f_F)\right) \tag{4}$$

where:

$$f_F = \sin(3\phi) \tag{5}$$

$$f_S = \cos(3\phi) \tag{6}$$

The peaks of curvature at the main scale occur for $\phi = \phi/2 + n\pi$ (Figure 2). Since the CWT peaks where the curvature peaks, we expect the location of meander nodes to correspond with the location of the meander apex. The third modes in equation (4) define the shape of the meander. For downstream skewed meanders we expect two peaks in the third mode at $\phi = 1/3\pi + n\pi$ and $\phi = 2/3\pi + n\pi$ with, respectively, an opposite and equal sign as the main-mode peak (Figure 2). For upstream skewed meanders these peaks are reversed. For fat meanders, two peaks occur at $\phi = 1/6\pi + n\pi$ and $\phi = 5/6 + n\pi$ with equal sign as the main-mode peak and one peak at $\phi = \pi/2 + n\pi$ with opposite sign as the main-mode (Figure 2). For an angular meander, these peaks are reversed. The angularity of a meander is used here to refer to meanders that have previously been named as "dog leg shaped," "male meanders," or "hairpin bends." As for the main-mode peak, we expect the third-mode peaks to correspond to small-scale peaking of the curvature in the half meanders.

The behavior of the third modes in the Kinoshita-generated curves is exploited to compute the shape parameters from the CWT. Given the meander node, the half meander spans a planform reach defined by the zero crossing lines at the meander period (section 2.4). The leftside of this meander reach is assigned $\phi = 0$ and

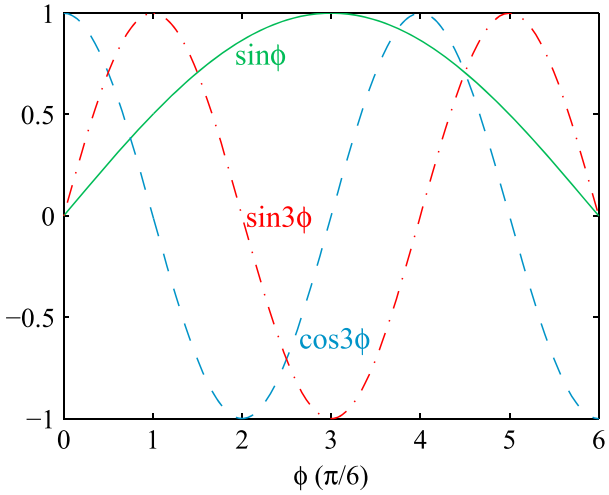

Figure 2. Trigonometric functions in equation (4) generating the main meander mode (green, solid line) and two third modes to include fattening (red, dash-dotted line) and skewing (blue, dashed line) for $\phi \in [0, \pi]$.

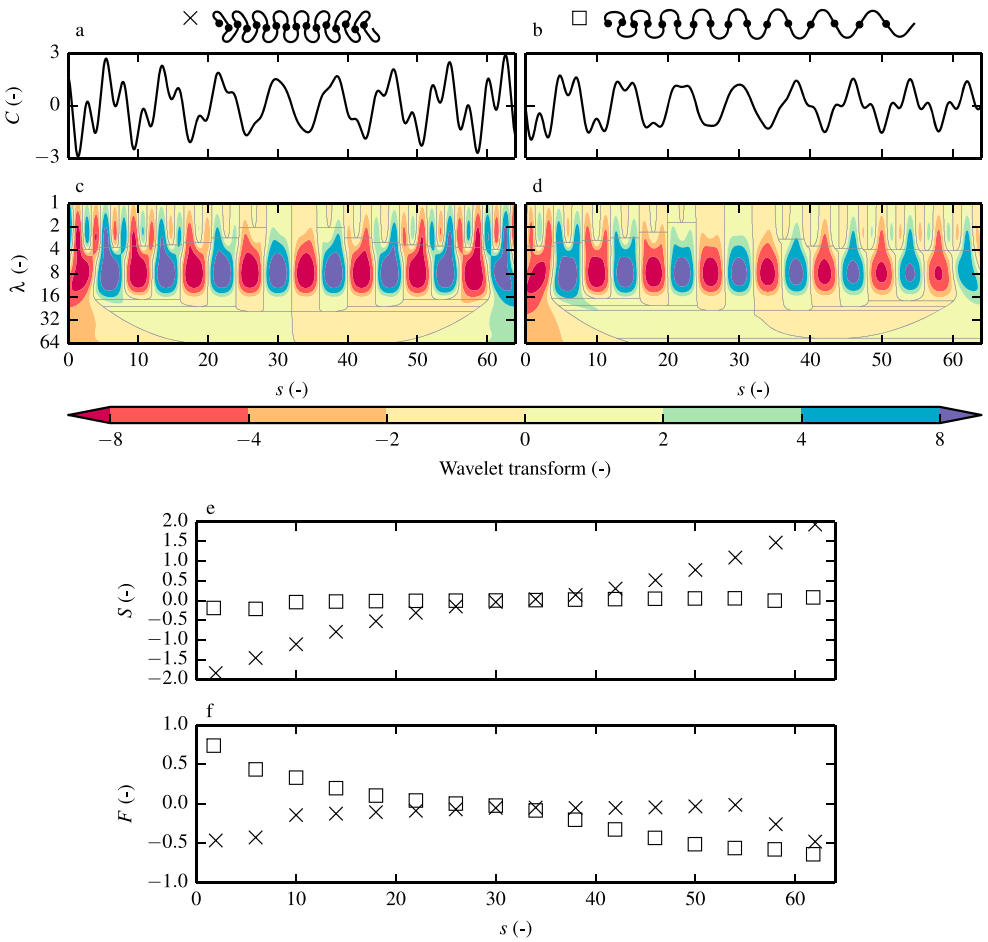

Figure 3. Two Kinoshita-generated planforms with the corresponding curvature series, (a) the first with gradual transition from upstream to downstream skewing and (b) the second one with gradual transition from fat meanders to angular meanders. (c and d) For both planforms the CWT is also shown as a contour. The vertical gray lines indicate the zero crossings of the CWT. The horizontal straight gray lines are the upper and lower boundaries of the scale space intervals corresponding to the tree nodes. The two planforms are characterized in the bottom two panels and are represented by crosses and squares for the planforms in Figures 3a and 3b, respectively. (e) The skewing parameter and (f) the fattening parameter.

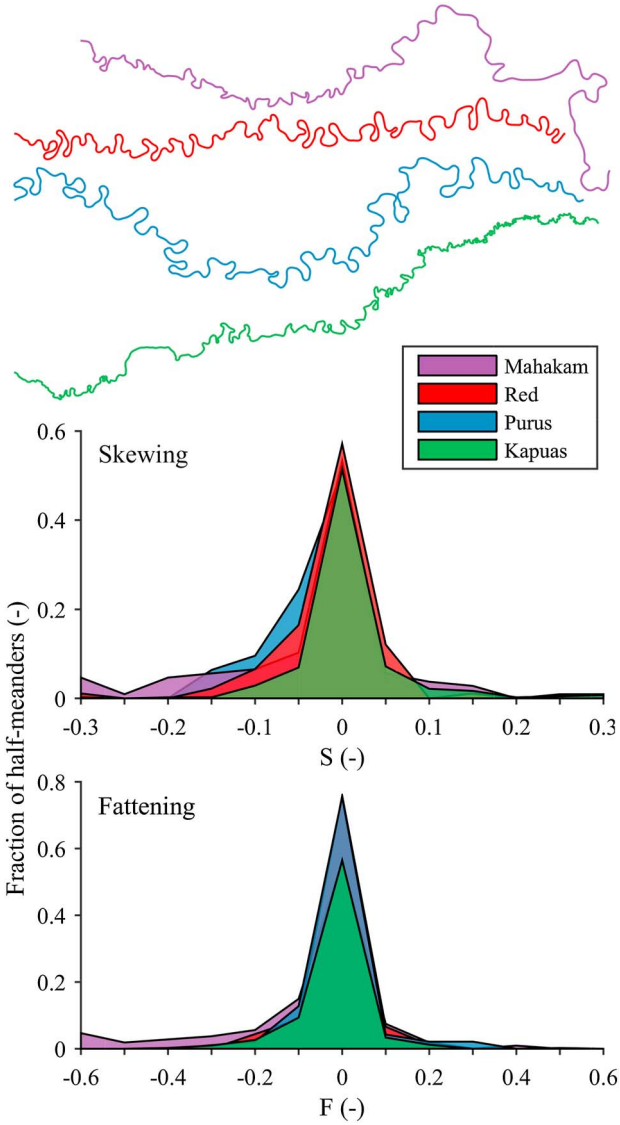

Figure 4. Histograms for the occurrence of (a) skewing and (b) fattening parameters for the Mahakam River (pink), Red River (red), Purus River (blue), and the Kapuas River (green).

the rightside $\phi = \pi$. The CWT at one third of the meander scale ($\Phi_s(\phi)$) defines the shape of the meander. Based on $\Phi_s(\phi)$ two shape parameters are defined:

$$\mathcal{S} = \frac{|\Phi_s|_{\max}}{\Phi_m} \frac{\int_0^\pi \Phi_s f_S \, d\phi}{\int_0^\pi f_S^2 \, d\phi} \sqrt{\frac{\delta s}{\sigma}} \tag{7}$$

$$\mathcal{F} = \frac{|\Phi_s|_{\max}}{\Phi_m} \frac{\int_0^\pi \Phi_s f_{\mathcal{F}} \, d\phi}{\int_0^\pi f_{\mathcal{F}}^2 \, d\phi} \sqrt{\frac{\delta s}{\sigma}} \tag{8}$$

where δs is the sampling interval of the centreline and σ is the scale at which the secondary wavelet transform is computed. The term $\sqrt{\delta s/\sigma}$ is needed to correct for sampling dependency of the shape parameters. Given the definition of f_S, when s is defined positive in downstream direction, a positive $\mathcal{S}$ corresponds to a downstream skewed meander, while a negative $\mathcal{S}$ corresponds to an upstream skewed meander. Similarly, a positive $\mathcal{F}$ corresponds to fat meanders, while a negative $\mathcal{F}$ corresponds to angular meanders.

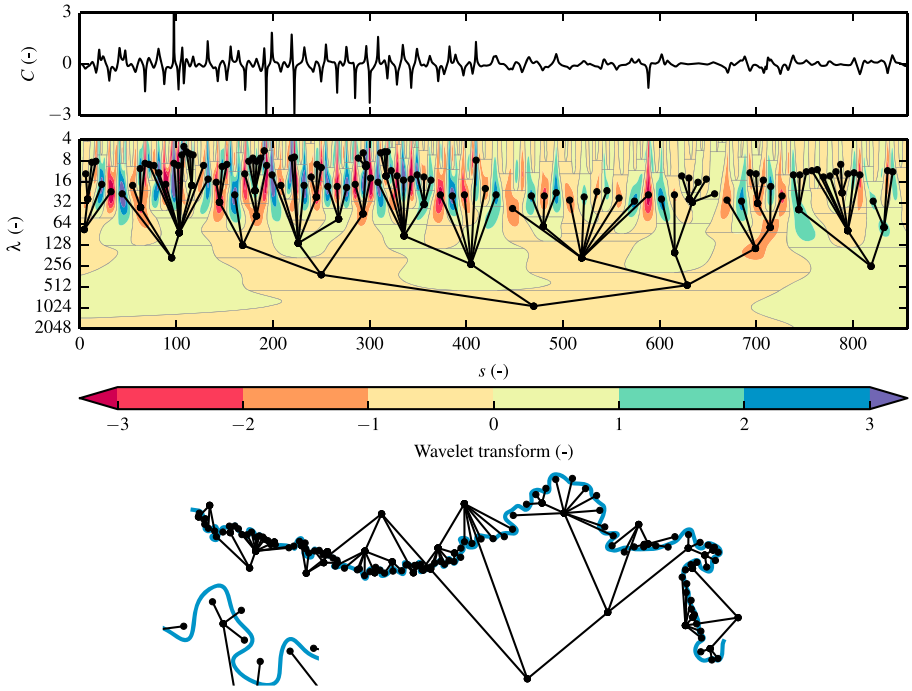

Figure 5. Multiple loop tree for the Mahakam River. The top panel shows the curvature series. In the middle panel the multiple loop tree is displayed on top of the CWT it was derived from. The vertical gray lines indicate the zero crossings of the CWT. The horizontal straight gray lines are the upper and lower boundaries of the scale space segments corresponding to the tree nodes. In the lower part the same tree is displayed in connection with the planform of the river. The position of each of the nodes is determined based on the corresponding scale and the center of curvature of the corresponding river reach. The small inset in the lower left corner shows a detail of the planform with a fat meander on the right and a double headed meander on the left. The double headed meander is identified as a complex of three meanders.

3. Results

3.1. Synthetic Rivers

Kinoshita-generated planforms are used to evaluate the performance of the shape parameters. Two planforms have been generated: one transitioning from upstream skewing to downstream skewing (Figure 3a) and one transitioning from fat meanders to angular meanders (Figure 3b). The wavelet spectra feature characteristic signatures typical for the different types of bends (Figures 3a and 3b). All half meanders have the wavelet peak at a wavelength corresponding to the meander wavelength. The peaks have alternating sign, coinciding with a curving of the planform to the right or to the left. At one third of the meander scale secondary peaks appear. For skewed and fat meanders there are always two equally signed peaks. For upstream skewed meanders a stronger peak is found at the upstream side, while for downstream skewed meanders this peak is found on the downstream side (Figure 3a). This results in a negative $\mathcal{S}$ for upstream skewed meanders and a positive $\mathcal{S}$ for downstream skewed meanders (Figure 3c). The location of the secondary peak for upstream or downstream skewed meanders always occurs at a fixed location with respect to the meander peak. This is a direct consequence of the phase locking in the Kinoshita curve. The intensity of the secondary peaks increases for increasing skewness.

Fat meanders feature two peaks in the CWT with almost equal intensity at a fixed location (Figure 3b). The intensity of the peaks directly relates to the intensity of fattening. Sharply curved meanders surrounded by straight reaches feature one peak at the same location and with the same sign as the main meander peak (Figure 3b). This results in positive values of $\mathcal{F}$ for fat meanders and negative values of $\mathcal{F}$ for sharp meanders (Figure 3d). Meanders in the central region of the two series have very low power in the secondary peaks, resulting in shape parameters close to zero (Figures 3c and 3d).

3.2. Real River Examples

The analysis is applied to the planform of four rivers: the Red River, the Purus River, the Mahakam River, and the Kapuas River. The Red River flows in a temperate region while the latter three in tropical regions.

Most meanders in the three rivers are neither skewed nor fat (Figure 4). All three rivers have mostly upstream skewed meanders, but the Red River also has some downstream skewed ones. Fattening is strongest in the Red River and the Purus River. Angularity (negative fattening) is strongest for the Mahakam River, which is known to feature sharp bends surrounded by relatively straight reaches (Figure 4c) [*Vermeulen et al.*, 2014, 2015].

The multiple looping tree reflects several scales of looping for the Mahakam River (Figure 5). The largest nodes in the tree reveal the large-scale structure of the Mahakam River which can be interpreted as the valley curvature induced by the local geology and topography [*Vermeulen et al.*, 2014]. These largest nodes have several child nodes corresponding to smaller structure looping. In some cases a multiple loop is composed of only three half meanders. This loop can be interpreted as double heading (see inset in Figure 5). The transition from a "fat" meander to a double headed meander is gradual. Its classification strongly depends on the scale at which the wavelet transform is strongest (see inset in Figure 5). As soon as the CWT power of the curvature fluctuation of the minor heads in a fat meander exceed the power at the meander scale, the minor heads become new half meanders, and the former meander bend becomes a multiple loop with three half meanders. The multiple loop trees of the Mahakam also reveal several multiple loops that gradually decrease in amplitude moving from upstream to downstream (Figure 5).

4. Conclusions

In this contribution we address the lack of an objective, quantitative method to characterize meandering which is able to include the multiscale nature and the nonstationarity of the phenomenon. The proposed method uses curvature series, analyzed with continuous wavelet transforms. The typical meander wavelength is determined, along with two parameters that quantify the shape of the meanders: skewing and fattening.

A tree is subsequently obtained for all supermeander scales, called the multiple loop tree. This tree describes the interrelation between all processes occurring at scales ranging from double heading up to valley curvature. Each node in the tree connects to nodes at smaller scales and represents a curving feature in the planform. The end nodes of the tree represent single half meanders which are interrelated through larger-scale features. The tree can be used to recognize patterns in the planform at different scales. The patterns at different scales can interact among each other [*Gutierrez and Abad*, 2014] and can potentially be matched with local geological confinement [*Frias et al.*, 2015; *Mendoza et al.*, 2016], vegetation, or other factors that influence meander formation.

The applicability of the method extends far beyond the fluvial case. It is applicable to all meandering structures such as lava flows, turbidity currents, tidal channels, rivulets, supraglacial streams, and extraterrestrial flows. The method has the potential to objectively compare meandering resulting from contrasting environmental factors and underlying processes.

Acknowledgments
This research was supported by the Royal Netherlands Academy of Arts and Sciences (KNAW), project SPIN3-JRP-29, and by NWO-WOTRO Science for Global Development, project WT76-269. We thank Meinhard Bayani Cardenas, the Associate Editor, Efi Foufoula-Georgiou, Jon Schwenk, and one anonymous reviewer for their comments and suggestions. The data used in this study can be obtained by contacting the corresponding author. The processing routines can be downloaded at https://github.com/bartverm/meanderscribe.git.

References

Abreu, V., M. Sullivan, C. Pirmez, and D. Mohrig (2003), Lateral accretion packages (LAPs): An important reservoir element in deep water sinuous channels, *Mar. Petrol. Geol.*, *20*(6–8), 631–648, doi:10.1016/j.marpetgeo.2003.08.003.

Andrle, R. (1996), Measuring channel planform of meandering rivers, *Phys. Geogr.*, *17*(3), 270–281, doi:10.1080/02723646.1996.10642585.

Baker, V. R. (2001), Water and the Martian landscape, *Nature*, *412*(6843), 228–236, doi:10.1038/35084172.

Beyer, G. (2003), Terrain inclination and curvature from wavelet coefficients, *J. Geod.*, *76*(9), 557–568, doi:10.1007/s00190-002-0278-1.

Brice, J. C. (1974), Evolution of meander loops, *Geol. Soc. Am. Bull.*, *85*(4), 581–586, doi:10.1130/0016-7606(1974)85<581:EOML>2.0.CO;2.

Fornari, D. (1986), Submarine lava tubes and channels, *Bull. Volcanol.*, *48*(5), 291–298, doi:10.1007/BF01081757.

Foufoula-Georgiou, E., and P. Kumar (1994), Wavelets in geophysics, in *Wavelet Analysis and Its Applications*, vol. 4, edited by C. K. Chui, Academic Press, Los Angeles, Calif.

Frias, C. E., J. D. Abad, A. Mendoza, J. Paredes, C. Ortals, and H. Montoro (2015), Planform evolution of two anabranching structures in the Upper Peruvian Amazon River, *Water Resour. Res.*, *51*, 2742–2759, doi:10.1002/2014WR015836.

Frothingham, K. M., and B. L. Rhoads (2003), Three-dimensional flow structure and channel change in an asymmetrical compound meander loop, Embarras River, Illinois, *Earth Surf. Processes Landforms*, *28*(6), 625–644, doi:10.1002/esp.471.

Greeley, R. (1971), Lunar Hadley rille: Considerations of its origin, *Science*, *172*(3984), 722–725, doi:10.1126/science.172.3984.722.

Güneralp, İ., and B. L. Rhoads (2011), Influence of floodplain erosional heterogeneity on planform complexity of meandering rivers, *Geophys. Res. Lett.*, *38*, L14401, doi:10.1029/2011GL048134.

Gutierrez, R. R., and J. D. Abad (2014), On the analysis of the medium term planform dynamics of meandering rivers, *Water Resour. Res.*, *50*, 3714–3733, doi:10.1002/2012WR013358.

Harden, D. R. (1990), Controlling factors in the distribution and development of incised meanders in the central Colorado Plateau, *Geol. Soc. Am. Bull.*, *102*(2), 233–242, doi:10.1130/0016-7606(1990)102<0233:CFITDA>2.3.CO;2.

Hardy, R. J., J. L. Best, S. N. Lane, and P. E. Carbonneau (2009), Coherent flow structures in a depth-limited flow over a gravel surface: The role of near-bed turbulence and influence of Reynolds number, *J. Geophys. Res.*, *114*, F01003, doi:10.1029/2007JF000970.

Harris, J., J. L. Hirst, and M. J. Mossinghoff (2008), *Combinatorics and Graph Theory*, Springer, New York.
Hooke, J. (1984), Changes in river meanders: A review of techniques and results of analyses, *Prog. Phys. Geogr.*, *8*(4), 473–508, doi:10.1177/030913338400800401.
Hooke, J. (2003), River meander behaviour and instability: A framework for analysis, *Trans. Inst. Br. Geogr.*, *28*(2), 238–253, doi:10.1111/1475-5661.00089.
Hooke, J. (2007), Complexity, self-organisation and variation in behaviour in meandering rivers, *Geomorphology*, *91*(3–4), 236–258, doi:10.1016/j.geomorph.2007.04.021.
Howard, A. D., and A. T. Hemberger (1991), Multivariate characterization of meandering, *Geomorphology*, *4*(3), 161–186, doi:10.1016/0169-555X(91)90002-R.
Jaffard, S. (1996), Trees in the time-scale domain, in *Trees, Prog. in Probab.*, vol. 40, edited by S. Jaffard, pp. 15–24, Birkhäuser, Basel, Switzerland, doi:10.1007/978-3-0348-9037-3_2.
Jaffard, S., B. Lashermes, and P. Abry (2007), Wavelet leaders in multifractal analysis, in *Wavelet Analysis and Applications*, edited by T. Qian, M. I. Vai, and Y. Xu, pp. 201–246, Birkhäuser, Basel, Switzerland, doi:10.1007/978-3-7643-7778-6_17.
Karlstrom, L., P. Gajjar, and M. Manga (2013), Meander formation in supraglacial streams, *J. Geophys. Res. Earth Surf.*, *118*, 1897–1907, doi:10.1002/jgrf.20135.
Keylock, C. J., A. Singh, and E. Foufoula-Georgiou (2014), The complexity of gravel bed river topography examined with gradual wavelet reconstruction, *J. Geophys. Res. Earth Surf.*, *119*, 682–700, doi:10.1002/2013JF002999.
Koenders, R., R. C. Lindenbergh, J. E. A. Storms, and M. Menenti (2014), Multiscale curvatures for identifying channel locations from DEMs, *Comput. Geosci.*, *68*, 11–21, doi:10.1016/j.cageo.2014.03.016.
Kolla, V., H. Posamentier, and L. Wood (2007), Deep-water and fluvial sinuous channels—Characteristics, similarities and dissimilarities, and modes of formation, *Mar. Pet. Geol.*, *24*(6–9), 388–405, doi:10.1016/j.marpetgeo.2007.01.007.
Komatsu, G., and V. R. Baker (1994), Meander properties of Venusian channels, *Geology*, *22*(1), 67–70, doi:10.1130/0091-7613(1994)022<0067:MPOVC>2.3.CO;2.
Kuijper, A. (2004), On detecting all saddle points in 2D images, *Pattern Recognit. Lett.*, *25*(15), 1665–1672, doi:10.1016/j.patrec.2004.06.017.
Lashermes, B., E. Foufoula-Georgiou, and W. E. Dietrich (2007), Channel network extraction from high resolution topography using wavelets, *Geophys. Res. Lett.*, *34*, L23S04, doi:10.1029/2007GL031140.
Lazarus, E. D., and J. A. Constantine (2013), Generic theory for channel sinuosity, *Proc. Natl. Acad. Sci. U.S.A.*, *110*(21), 8447–8452, doi:10.1073/pnas.1214074110.
Le Grand-Piteira, N., A. Daerr, and L. Limat (2006), Meandering rivulets on a plane: A simple balance between inertia and capillarity, *Phys. Rev. Lett.*, *96*, 254503, doi:10.1103/PhysRevLett.96.254503.
Lindeberg, T. (1990), Scale-space for discrete signals, *IEEE Trans. Pattern Anal. Mach. Intell.*, *12*(3), 234–254, doi:10.1109/34.49051.
Lowe, D. G. (1989), Organization of smooth image curves at multiple scales, *Int. J. Comput. Vision*, *3*(2), 119–130, doi:10.1007/BF00126428.
Mackworth, A. K., and F. Mokhtarian (1988), The renormalized curvature scale space and the evolution properties of planar curves,paper presented at CVPR '88 Computer Society Conference on Computer Vision and Pattern Recognition, pp. 318–326, Ann Arbor, Michigan, 5–9 Jun., doi:10.1109/CVPR.1988.196255.
Malin, M. C., and K. S. Edgett (2003), Evidence for persistent flow and aqueous sedimentation on early Mars, *Science*, *302*(5652), 1931–1934, doi:10.1126/science.1090544.
Mallat, S. (1991), Zero-crossings of a wavelet transform, *IEEE Trans. Inf. Theory*, *37*(4), 1019–1033, doi:10.1109/18.86995.
Marani, M., S. Lanzoni, D. Zandolin, G. Seminara, and A. Rinaldo (2002), Tidal meanders, *Water Resour. Res.*, *38*(11), 1225, doi:10.1029/2001WR000404.
Mendoza, A., J. Abad, C. Frias, C. Ortals, J. Paredes, H. Montoro, J. Vizcarra, C. Simon, and G. Soto-Cortés (2016), Planform dynamics of the Iquitos anabranching structure in the Peruvian upper Amazon river, *Earth Surf. Processes Landforms*, doi:10.1002/esp.3911, in press.
Mokhtarian, F., and A. Mackworth (1992), A theory of multiscale, curvature-based shape representation for planar curves, *IEEE Trans. Pattern Anal. Mach. Intell.*, *14*(8), 789–805, doi:10.1109/34.149591.
Motta, D., J. D. Abad, E. J. Langendoen, and M. H. García (2012), The effects of floodplain soil heterogeneity on meander planform shape, *Water Resour. Res.*, *48*, W09518, doi:10.1029/2011WR011601.
Motta, D., E. J. Langendoen, J. D. Abad, and M. H. García (2014), Modification of meander migration by bank failures, *J. Geophys. Res. Earth Surf.*, *119*, 1026–1042, doi:10.1002/2013JF002952.
Mount, N. J., N. J. Tate, M. H. Sarker, and C. R. Thorne (2013), Evolutionary, multi-scale analysis of river bank line retreat using continuous wavelet transforms: Jamuna River, Bangladesh, *Geomorphology*, *183*, 82–95, doi:10.1016/j.geomorph.2012.07.017.
Muzy, J. F., E. Bacry, and A. Arneodo (1991), Wavelets and multifractal formalism for singular signals: Application to turbulence data, *Phys. Rev. Lett.*, *67*, 3515–3518, doi:10.1103/PhysRevLett.67.3515.
Muzy, J. F., E. Bacry, and A. Arneodo (1993), Multifractal formalism for fractal signals: The structure-function approach versus the wavelet-transform modulus-maxima method, *Phys. Rev. E*, *47*, 875–884, doi:10.1103/PhysRevE.47.875.
Nicolleau, F., and J. C. Vassilicos (1999), Wavelets for the study of intermittency and its topology, *Philos. Trans. R. Soc. A*, *357*(1760), 2439–2457, doi:10.1098/rsta.1999.0441.
O'Neill, M. P., and A. D. Abrahams (1986), Objective identification of meanders and bends, *J. Hydrol.*, *83*(3–4), 337–353, doi:10.1016/0022-1694(86)90160-5.
Parker, G., K. Sawai, and S. Ikeda (1982), Bend theory of river meanders. Part 2: Nonlinear deformation of finite-amplitude bends, *J. Fluid Mech.*, *115*, 303–314, doi:10.1017/S0022112082000767.
Parker, G., P. Diplas, and J. Akiyama (1983), Meander bends of high amplitude, *J. Hydraul. Eng.*, *109*(10), 1323–1337, doi:10.1061/(ASCE)0733-9429(1983)109:10(1323).
Peakall, J., B. McCaffrey, and B. Kneller (2000), A process model for the evolution, morphology, and architecture of sinuous submarine channels, *J. Sediment. Res.*, *70*(3), 434–448, doi:10.1306/2DC4091C-0E47-11D7-8643000102C1865D.
Rinaldi, M., and P. A. Johnson (1997), Characterization of stream meanders for stream restoration, *J. Hydraul. Eng.*, *123*(6), 567–570, doi:10.1061/(ASCE)0733-9429(1997)123:6(567).
Rosin, P. L. (1998), Determining local natural scales of curves, *Pattern Recognit. Lett.*, *19*(1), 63–75, doi:10.1016/S0167-8655(97)00158-X.
Schumm, S. A. (1967), Meander wavelength of alluvial rivers, *Science*, *157*(3796), 1549–1550, doi:10.1126/science.157.3796.1549.
Schwenk, J., S. Lanzoni, and E. Foufoula-Georgiou (2015), The life of a meander bend: Connecting shape and dynamics via analysis of a numerical model, *J. Geophys. Res. Earth Surf.*, *120*, 690–710, doi:10.1002/2014JF003252.
Seminara, G. (2006), Meanders, *J. Fluid Mech.*, *554*, 271–297, doi:10.1017/S0022112006008925.
Seminara, G., G. Zolezzi, M. Tubino, and D. Zardi (2001), Downstream and upstream influence in river meandering. Part 2: Planimetric development, *J. Fluid Mech.*, *438*, 213–230, doi:10.1017/S0022112001004281.

Stark, C. P., J. R. Barbour, Y. S. Hayakawa, T. Hattanji, N. Hovius, H. Chen, C.-W. Lin, M.-J. Horng, K.-Q. Xu, and Y. Fukahata (2010), The climatic signature of incised river meanders, *Science*, *327*(5972), 1497–1501, doi:10.1126/science.1184406.

Thompson, A. (1986), Secondary flows and the pool-riffle unit: A case study of the processes of meander development, *Earth Surf. Processes Landforms.*, *11*(6), 631–641, doi:10.1002/esp.3290110606.

Torrence, C., and G. P. Compo (1998), A practical guide to wavelet analysis, *Bull. Am. Meteorol. Soc.*, *79*(1), 61–78, doi:10.1175/1520-0477(1998)079<0061:APGTWA>2.0.CO;2.

van Gerven, L., and A. J. F. Hoitink (2009), Analysis of river planform geometry with wavelets: Application to the Mahakam River reveals geographical zoning, in *River, Coastal and Estuarine Morphodynamics. RCEM2009. Santa Fe City, Argentina*, edited by C. Vionnet et al., CRC Press, Boca Raton, Fla.

Vermeulen, B., A. J. F. Hoitink, S. W. van Berkum, and H. Hidayat (2014), Sharp bends associated with deep scours in a tropical river: The river Mahakam (East Kalimantan, Indonesia), *J. Geophys. Res. Earth Surf.*, *119*, 1441–1454, doi:10.1002/2013JF002923.

Vermeulen, B., A. J. F. Hoitink, and R. J. Labeur (2015), Flow structure caused by a local cross-sectional area increase and curvature in a sharp river bend, *J. Geophys. Res. Earth Surf.*, *120*, 1771–1783, doi:10.1002/2014JF003334.

Witkin, A. P. (1984), Scale-space filtering: A new approach to multi-scale description, in *Acoustics, Speech, and Signal Processing, IEEE International Conference on ICASSP '84*, vol. 9, pp. 150–153, IEEE, doi:10.1109/ICASSP.1984.1172729.

Yuan, Y., H. Wei, L. Zhao, and Y. Cao (2009), Implications of intermittent turbulent bursts for sediment resuspension in a coastal bottom boundary layer: A field study in the western Yellow Sea, China, *Mar. Geol.*, *263*(1–4), 87–96, doi:10.1016/j.margeo.2009.03.023.

Yuille, A. L., and T. A. Poggio (1986), Scaling theorems for zero crossings, *IEEE Trans. Pattern Anal. Mach. Intell.*, *18*(1), 15–25, doi:10.1109/TPAMI.1986.4767748.

Zolezzi, G., and İ. Güneralp (2015), Continuous wavelet characterization of the wavelengths and regularity of meandering rivers, *Geomorphology*, *252*, 98–111, doi:10.1016/j.geomorph.2015.07.029.